Dating submarine landslides using the transient response of gas hydrate stability

Alexey Portnov (portnovalexey@gmail.com)
University of Texas https://orcid.org/0000-0003-4930-8308
Kehua You
University of Texas
Peter Flemings
The University of Texas at Austin https://orcid.org/0000-0002-5377-3694
Ann Cook
The Ohio State University
Mahdi Heidari
University of Texas
Derek Sawyer
The Ohio State University https://orcid.org/0000-0002-0779-7775

Article

Keywords:

Posted Date: December 3rd, 2021

DOI: https://doi.org/10.21203/rs.3.rs-1125310/v1

Abstract

Submarine landslides are prevalent on the modern-day seafloor, yet an elusive problem is constraining the timing of slope failure. Herein, we present a novel technique for constraining the age of submarine landslides without sediment core dating. Underneath a submarine landslide in the Orca Basin, Gulf of Mexico, in 3D seismic data we map an irregular bottom simulating reflection (BSR), which mimics the geometry of the pre-slide seafloor rather than the modern bathymetry. Based on the observed BSR, we suggest that the gas hydrate stability zone (GHSZ) is currently adjusting to the post-slide sediment temperature perturbations. We apply transient conductive heat flow modeling to constrain the response of the GHSZ to the slope failure, which yields a most likely age of ~8 ka demonstrating that gas hydrate systems can respond to slope failures even on the millennia timescales. We also provide an analytical approach to rapidly determine the age of submarine slides at any location.

Main Text

Submarine slope failures are hazardous mass transport events that can mobilize tens and hundreds of cubic kilometers of sediments in a matter of hours[1–4]. Submarine slides can cause destructive tsunamis and damage to costly seabed infrastructure, yet the causes of these events are often unknown[3,5–8]. Although submarine slides have never been observed directly, seafloor scars and mass transport deposits (MTDs) from the slope failures are detectable through seismic networks, seabed bathymetry and 3D seismic surveys[9,10].

Important factors that contribute to submarine slope instability are tectonic activity, excess pore pressure, and the development of weak layers in marine sediments[3,4,11]. These mechanisms may reactivate during certain geologic events, therefore defining the age of a landslide can help constrain potential triggers (e.g. rapid sea level changes, glacial-interglacial cycles, periods of enhanced sedimentation, and earthquakes)[5,12–15]. Defining the origin and repeatability of slope failures requires more extensive and accurate slide dating[14]. Slide age can be determined using various sediment dating approaches; however, this is often limited by the availability of sediment cores. Additionally, limitations of the dating methods and inaccurate location of the dated sediment samples can result in significant uncertainties reaching several thousand years [12,14]. Our study uses a new approach that does not require sediment core data, instead, we use bottom simulating reflections (BSRs) mapped in 3D seismic data to determine a landslide age.

BSRs are commonly observed in marine reflection seismic data and are associated with natural gas hydrate accumulations[16,17]. Gas hydrates, solid compounds of water and gas, are widespread in marine sediments within the gas hydrate stability zone (GHSZ)[18,19]. On tropical and temperate margins, hydrates become stable in shallow sediments under water column depths of >500 m. BSRs are non-stratigraphic reflections at the base of the GHSZ originating from a sharp acoustic impedance change primarily due to

the accumulation of free gas below the BSR [16]. The base of the GHSZ is a sensitive interface controlled by a combination of four factors: pressure, temperature, gas composition, and pore water salinity[18,20].

Typically, the four factors remain regionally uniform and the BSR parallels the seafloor gently deepening with increasing water depth, which causes an increase in hydrostatic pressure[17]. Yet, there are irregular BSRs that deviate from the seafloor bathymetry. Such BSRs indicate there may be lateral changes in the temperature gradient[21–23], gas composition[24] or salinity[25]. Although less common, BSRs can appear as multiple reflections named double BSRs, possibly indicating presence of thermogenic gas[26–28], high sedimentation rates, and/or recent tectonic shifts[29–31].

Here, we analyze an irregular BSR underlying a landslide scarp and MTD in the Orca Basin, Gulf of Mexico. The BSR in this location deviates from the modern seafloor bathymetry due to slide-induced temperature perturbations imposed upon the sediments. We determine the age of the submarine landslide using the deviation of the observed BSR from its steady-state depth, the reconstructed pre-slide bathymetry, the modeled post-slide sediment temperature and gas hydrate stability.

Geologic Setting

The Orca Basin in the Gulf of Mexico is a salt-withdrawal minibasin that is well known for a large (123 km^2) anoxic hypersaline brine pool occurring at the bottom of the basin[32]. The water depths in the basin range from 1600 to 2600 m (Figure 1A). The seafloor of the Orca Basin is marked by prominent escarpments and rugged topography resulting from slump deposits and rafted blocks produced by multiple submarine slide events[33,34] (Figure 1A, B).

Our study area is located at the southern flank of the Orca Basin where a sharp ~ 90 m tall seafloor escarpment marks the head of a submarine slide described in a previous study [33] (Figure 1A). The slide area exhibits an ~3 x 7.5 km excavation underlain by a salt body. Previous study also reported an accumulation of MTDs at the basin floor that were sourced from the slides above [33](Figure 1A, B). The BSR was previously mapped [35] and further analyzed in this study over an area of 44.3 km^2 (Figure 1C). Gas hydrates were also identified in industry wells flanking the escarpment (Figure 1D).

Irregular BSR In The Orca Basin

In the depth-migrated 3D seismic data, we observe multiple negative-amplitude BSRs that crosscut stratigraphy (Figure 1D, 2A). The BSRs are distinct and located at depths between 2300-3500 meters below sea level (mbsl) (230-1130 meters below seafloor (mbsf) (Figure 1C). The large BSR depth range is surprising given that BSRs are typically subparallel to the seafloor. The irregular BSR configuration is especially well-observed along seismic section c-d extending across the southern rim and slope of the Orca Basin (Figure 2A, B). The shallowest BSR occurs within the slide escarpment area upslope (~200 mbsf) and the deepest BSR occurs below the MTD downslope (~1110 mbsf) (Figure 2A, B).

There are several possible explanations for the southward shallowing BSRs. First, it could be caused by the higher sediment temperature over the heat-conductive salt body; this would drive the base of the GHSZ shallower. Similar effects have been previously analyzed within the roofs of salt bodies[37–39]. The geothermal gradients required to explain the depths of the observed BSR along the profile c-d show a significant increase from 16.3°C/km downslope to as high as 43°C/km above the salt summit (Figure 2A, see methods).

The second explanation is based on the fact that the BSR is in a striking agreement with the reconstructed pre-slide bathymetry of the Orca Basin southern rim (Figure 2A, B, see methods). The observed BSR lies at an approximately constant depth below the reconstructed pre-slide seafloor both, within the slide escarpment upslope and downslope, where the pre-slide seafloor submerges along the base of the MTD (Figure 2A, B). Such a configuration is observed over a wide area as illustrated by the thickness maps (Figure 1C). The thickness between the BSR and the pre-slide seafloor (~400-550 m) is more uniform over the study area as compared to the thickness between the BSR and the modern seafloor (~230-1130 m). This suggests the base of the GHSZ in the Orca Basin still closely reflects the pre-slide seafloor configuration.

To understand the temperature effect of the salt body on the observed BSR shape, we constrain the regional average geothermal gradient and run a 2D conductive heat flow model along profile c-d (Figure 1). We then model the response time of the GHSZ to the slide-induced sediment temperature change and compare the results with the observed BSR depth to define the age of the slope failure.

Results And Discussion

The regional average geothermal gradient of 25.5°C/km is derived from the three BSR depths where sediment temperature is assumed to be at steady-state: away from the heat-conductive shallow salt, outside of the slide escarpment and outside of the MTD (red, yellow and white stars in the inset of Figure 2A). The 2D heat flow model shows a pronounced heat flow increase directly above the top of salt and elevated heat flow ~4000 m southward and northward along the profile c-d (Figure 3, see methods). The geothermal gradient predicted by the 2D heat flow model over the salt body is 30°C/km, and it gradually decreases to the average regional 25.5°C/km ~4000 m northward from the salt summit (Figure 3). However, these variations are insufficient to explain the shape of the irregular BSR, which requires geothermal gradients increasing from 16.3°C/km downslope to as high as 43°C/km above salt (Figure 2A).

Moreover, the 2D heat flow model predicts where the base of GHSZ would be at steady-state, and indicates that the sediments are still undergoing the residual post-slide temperature adjustment (Figure 3). To analyze this adjustment, profile c-d can be divided into three areas (Figure 2B): 1) the upslope area where the removal of the overburden is cooling the shallow sediments and drives the base of GHSZ down (Figure 2B, Figure 3), 2) the downslope area where the warming effect due to the deposition of the MTD drives the base of GHSZ upward, and 3) the areas outside of the MTD and slide escarpment where the

GHSZ is relatively steady-state (Figure 2B, Figure 3). The fact that the BSR still closely mimics the pre-slide seafloor implies that the temperature adjustment is not yet significant, and that the landslide is relatively young. The following time-transient heat flow model provides constraints on the age of the slope failure.

1D Transient Heat Flow Models

We model the transient post-slide temperature field at the upslope slide location where sediments experience cooling, and at the downslope MTD location, where the sediments undergo warming (Figure 2A, B, see methods). We use a bottom water temperature of 4.2°C for the upper boundary condition. To constrain the lower boundary at each location, we apply constant heat flow that corresponds to the steady-state geothermal gradients predicted by the 2D heat flow model: 30°C/km at the upslope location and 25.5°C/km at the downslope location (Figure 3). Based on the 1D heat flow modeling (see equation (1) in methods), we define the transient temperature changes in the sediment column and derive the temperature profiles at certain times (time-temperature profiles) after the slide for both locations (see methods). Finally, to define the age of the slide event in the Orca Basin, we find the crossover of the three functions: the methane phase boundary curve, the observed BSR depth (reflecting the modern temperature), and the corresponding time-temperature profile (insets of Figure 2B).

2D steady-state conductive heat flow model used to estimate the effect of the salt body on the geothermal gradients along seismic section c-d (located in Figure 1). The model domain is 14 km deep and 16.5 km wide with constant basal heat flow. The properties of the sediment (i.e. thermal conductivity) vary with porosity and the properties of the salt vary with temperature (see methods and supplementary material). The model predicts an elevated geothermal gradient over salt (~30°C/km) and regional average geothermal gradient below the MTD (~25.5°C/km), which is however insufficient to explain the observed shift in the BSR in the Orca Basin (Figure 2A). We use the observed gradients at the upslope (30°C/km) and downslope (25.5°C/km) locations for our one-dimensional simulations (Figure 4).

Upslope Location

Given the 30°C/km steady-state geothermal gradient, the pre-slide temperature at the level of the modern seafloor (~220 meters below the pre-slide seafloor) was 10.7°C (Figure 4A). After the instantaneous ~220-meter seafloor drop caused by the slide, these warmer sediments were exposed to cooler bottom waters with a temperature 4.2°C (Figure 4A). Over thousands of years, the temperature within the subseafloor sediments gradually cools to adjust to the new boundary condition as shown by the time-temperature profiles (Figure 4A).

Based on the steady-state geothermal gradient, the pre-slide BSR would have been at ~ 465 m below the pre-slide seafloor (~245 meters relatively to the modern seafloor) (Figure 4a, black 0 kyr profile), and it will reach its post-slide steady-state depth at ~505 mbsf approximately 200 kyr after the slide event. Time-temperature profiles show the base of the GHSZ approaches approximately half-way to its steady-state depth during the first ~20 kyrs after the slope failure. Figure 4a shows that the intersection of the modern

BSR (~342 mbsf, blue line in Figure 4a) and methane phase boundary curve corresponds to the ~8 kyr time-temperature profile (red curve in Figure 4A), which constrains the upslope location age estimate for the Orca submarine slide.

Downslope Location

At the downslope location, we model a 400-meter thick sediment mass added to the top of the pre-slide seafloor to simulate the deposition of the MTD (Figure 4B). The initial temperature profile within the MTD is somewhat ambiguous because slope failure is a chaotic process involving sediment redeposition and unpredictable rates of mixing with the cold bottom water. We select a uniform 7.5°C temperature throughout the MTD for the model, which was the mean temperature in the ~220 m thick upslope sediment column prior to failure (Figure 2B, 4B). The temperature at the top of the MTD is 4.2°C.

The model shows that at the downslope location the depth of the pre-slide BSR was ~720 meters below the pre-slide seafloor (~1120 mbsf) (Figure 4B). It will reach its post-slide steady-state depth at 680 mbsf approximately 250 kyrs after the slide event, whereas complete steady state will be reached in ~350 kyrs (Figure 4B). The modern BSR is observed in the seismic data at ~1090 mbsf, which is only 30 m above its pre-slide location (Figures 3, 4B). The modern BSR depth and methane phase boundary intersection corresponds to the ~14 kyr time-temperature profile (red line in Figure 4B), which constrains the downslope location age estimate for the Orca submarine slide.

A) Transient 1D heat flow modeling at the upslope location (Figure 2B) showing the time-temperature profiles after the slope failure (removal of overburden). The figure shows the intersection of methane phase boundary (black curve) and modern BSR depth (blue line) corresponds to an 8 kyr time-temperature profile (red line) indicating the age of the Orca slide derived from the upslope location. B) Transient 1D heat flow modeling at the downslope location (Figure 2B) showing the time-temperature profiles after the MTD deposition. The model shows that the intersection of methane phase boundary (black curve) and modern BSR depth (blue line) corresponds to a 14 kyr time-temperature profile (red line). For the upper boundary condition, we use a bottom water temperature of 4.2°C. At the lower boundary, we apply constant heat flow that corresponds to 30°C/km geothermal gradient at the upslope location and 25.5°C/km at the downslope location (see supplementary material for thermal conductivity and diffusivity depth profiles). Front panel shows that both slide ages determined for the Orca Basin correlate with a rapid post-glacial sea level rise[40], which could cause increased slope instability across the worldwide continental margins[13].

Age Of The Orca Submarine Slide

At the upslope location, we predict an age of ~8 ka for the Orca submarine slide, whereas at the downslope location we predict an age of ~14 ka. We consider the 8 ka age estimate to be more accurate for two reasons. First, sediment removal upslope was likely a single fast-moving event. In contrast, the MTD at the downslope location may be an amalgamation of several landslides that occurred around the rim of the Orca basin [33]. Thus, the temperature profile within the sediments at the downslope may record

a number of slides, some older than the one released at the upslope location. Second, the depth interval between the pre-slide and modern BSR is wider and shallower at the upslope location compared to the downslope location (Figure 4A, B). Within this interval upslope, the thermal signal propagates faster resulting in the wider-spaced time-temperature profiles. Thus, the upslope location provides better age resolution than the densely clustered profiles at the downslope location.

The impact of slope failures on gas hydrate accumulations is different in the interval below the MTD than below the slide escarpments. Below the MTDs, there would be gas hydrate dissociation as the base of GHSZ rises with the temperature increase (Figure 2B). Gas hydrate dissociation below the MTDs (i.e. the downslope location) is an endothermic reaction[41] that would draw the heat from the sediments, slow the general warming trend, and consequently increase the modeled slide age. In contrast, below the slide escarpments (i.e. the upslope location), the deepening GHSZ entraps the underlying gas, which forms hydrate (Figure 2B). Gas hydrate formation is an exothermic process accompanied by heat release, which may slow the general cooling trend and likewise increase the modeled slide age. Therefore, the ~8 ka is the youngest age estimate for the Orca landslide. Accurate quantitative characterization of hydrate formation and dissociation depends on gas hydrate and gas saturations over the area, which are not available. In any case, our modeling shows that the effect of slope failures on gas hydrate systems can continue over tens of thousands of years after the slide events.

Our inferred age of the Orca slide (~8 ka) coincides with the final stage of rapid late Pleistocene–early Holocene sea level rise in the Gulf of Mexico averaging at ~12 mm/yr between 14.5 and 8 ka[40](inset of Figure 4B). An earlier study showed that this fast post-glacial sea-level rise could induce seismicity along faults on passive continental margins and increase the frequency of submarine slides worldwide[13] (inset of Figure 4). A similar mechanism could be responsible for the activation of deep-rooted and supra-salt faults, triggering submarine slides in the Gulf of Mexico, including the Orca Basin.

Model Sensitivity

Our landslide age estimates may be affected by factors that control gas hydrate stability, such as the presence of heavy hydrocarbons (ethane, propane, butane, pentane), and high salinity. In addition, geologic factors can also influence hydrate stability by altering temperature and pressure, such as elevated post-slide sedimentation rates and eustatic sea level change. These factors can contribute to the depth of the GHSZ, yet the impact on our age estimates is unlikely to be significant.

First, the presence of heavy hydrocarbons and/or elevated salinity in the shallow subseafloor sediments would provide the opposite effects at the upslope and downslope locations. Higher salinity would shift the methane hydrate phase boundary leftward in Figure 4 and result in a younger modeled slide age at the downslope location and older slide age at the upslope location. The presence of heavy hydrocarbons would shift the methane-hydrate phase boundary rightward in Figure 4 and result in the older modeled slide age at the downslope locations and younger age upslope. Neither salinity anomalies nor thermogenic gas are supported by our well log and seismic data.

Second, the high post-slide sediment deposition rate would result in a younger modeled slide age at the downslope location and older age at the upslope location. Based on the 3D seismic data, the hemipelagic drape within the slide escarpment is absent or <8 m thick, indicating that the effect of the sediment deposition is negligible. Additionally, the thin layer of post-slide sediments supports the relatively young age of the slide.

Third, the post-glacial sea level rise in the Gulf of Mexico[40] would only result in <7 m uncertainty in the pre-slide base of GHSZ based on the corresponding shift of the methane-hydrate phase boundary profile. This slightly affects the pre-slide BSR location but provides negligible effect on the slide age.

Universal Approach To Submarine Slide Dating Using BSRs

Equation (2) (see methods) provides a simple analytical method for a quick-look slide age (t_{slide}, s) estimate using the modern BSR depth (z_{bsr}, m) below slide escarpments (similar to the Orca upslope location) with a known temperature at the BSR depth (T_{bsr})(Figure 2A). We further find that parameter $\frac{z_{bsr}-z_{bsr,o}}{z_{bsr,1}-z_{bsr,o}}$ can be used to quantify the fractional heat dissipation after the slide, with a value of zero referring to the initial condition immediately after the slide and a value of 1 referring to the post-slide steady state (Figure 4A, 5). The plots of the fractional heat dissipation ($\frac{z_{bsr}-z_{bsr,o}}{z_{bsr,1}-z_{bsr,o}}$) versus the dimensionless time ($\frac{\kappa t}{z^2 bsr}$) all fall into one curve at different locations with different water depths, temperature gradients, thermal diffusivities, BSR temperatures and/or landslide thicknesses (Figure 5: red curve). This means that the age of a submarine landslide t_{slide}can be estimated simply from the diagram shown in Figure 5 with easily accessible parameters (z_{bsr}, $z_{bsr,o}$, $z_{bsr,1}$, κ). It is evident that the BSR shift from the pre-slide to post-slide steady-state ($z_{bsr,1} - z_{bsr,o}$) can be roughly equated to the thickness of a submarine slide (Figure 4A, 5).

The analytical solution (see equation (2) in methods), which estimates submarine slide age using BSR depths under the landslide escarpments, similar to the upslope location at Orca. z_{bsr} is calculated from equation (2) by assuming a constant, known temperature at the BSR depth (T_{bsr}) during the evolution. $z_{bsr,0}$ is the depth of a pre-slide steady-state BSR that can be estimated based on the thickness of removed sediments; $z_{bsr,1}$ is the depth of a post-slide steady-state BSR; κ is the average thermal diffusivity of the subseafloor sediment (see supplementary material); t_{slide} is the age of a submarine landslide. The analytical solution for the Orca upslope location using 30°C/km geothermal gradient (red dashed arrows) dates the slide to ~7.8 ka, which is similar to the result of our numerical simulation. Gray dashed lines show the sensitivity of the analytical solution to the varying geothermal gradients.

The age of the Orca slide from the analytical solution is ~7.8 ka, which is in a good agreement with our numerical solution (Figure 5). The discrepancy between the analytical and numerical solutions may be caused by a difference in domains; the numerical solution is solved for a finite domain, whereas the analytical solution is solved for a semi-infinite domain. There are also slightly different physical

properties with depth that could cause variation in the results as the numerical solution has varying porosity and thermal diffusivity, whereas the analytical solution assumes homogeneous sediments properties with depth.

Our seismic and modeling-based landslide dating technique is a novel method for dating submarine landslides without core data. Because gas hydrate systems occur worldwide and often coexist with submarine landslides, there may be many locations where our approach can be applied. Moreover, this technique is especially relevant given the expanding public seismic databases worldwide. The following are only few examples where published seismic data appear to show irregular BSRs deviating from the seafloor bathymetry below the landslide escarpment and/or below MTDs: the Cape Fear slide complex offshore the US East Coast [42], offshore Oregon, USA [43], the Storegga slide offshore southern Norway[44], the Brunei slide offshore Brunei[45], and the Hinlopen megaslide offshore Svalbard[46,47].

Conclusions

We estimate the age of the submarine landslide on the southern bank of the Orca Basin to be ~8 ka based on the modern depth of the bottom simulating reflection in seismic data coupled with numerical heat flow models. This new approach does not require seismic stratigraphic correlations or sediment core dating. We also provide an analytical solution that can be used for quick-look submarine slide age estimates elsewhere. Our study shows that the Orca and similar gas hydrate systems expand below the slide escarpments and dissociate below the MTDs. Finally, we find such transformations can be still ongoing thousands of years after the slope failures indicating long-lasting dynamic behavior of slide-impacted gas hydrate systems.

Methods

3D seismic data and pre-slide seafloor reconstruction

The seafloor, BSR, and salt surface are mapped in the 3D seismic data sampled to 4.8 m. We use depth-migrated 3D seismic data, which was originally converted from time to depth by WesternGeco. The seismic data provide accurate depths within the GHSZ (our target interval), which is supported by a good correlation between the depths of major seismic horizons (e.g. seafloor and salt top) and corresponding responses in resistivity and gamma ray well logs available in the study area. The frequency of the processed seismic data ranges from 5-55 Hz providing ~7-9 m vertical resolution at the BSR level.

We use the seafloor seismic reflection to reconstruct the pre-slide seafloor geometry and infer the base of the GHSZ before the slide event. For this reconstruction, we use manual and automatic interpolation of the bathymetric contours from the seafloor surface surrounding each headwall scarp. The approach provides a reasonable estimate of the change in water depth after the slide event and with it, the total volume of the slide (Figure 1B, Figure 2A, B). Under the basin floor, we extend the pre-slide seafloor

surface along the base of the MTD marked by a distinct trough-leading reflector indicating more consolidated slide sediments onlapping the ancient seafloor (Figure 2A).

Gas hydrate stability and geothermal gradients

The gas hydrate phase boundary was estimated assuming 100% methane concentration, 3.5% NaCl, and hydrostatic pressure [48]. The assumption of pure methane gas is supported by the seismic data showing no deep-rooted gas chimneys that could source heavier hydrocarbons towards the base of the GHSZ. To estimate the mean geothermal gradient, we apply linear temperature approximation between the seafloor and the BSR, using a bottom water temperature of 4.2°C, the BSR depth, and the methane hydrate phase boundary diagram.

2D heat flow modeling across the slope

We use a 2D plane-strain finite-element model to simulate the potential effect of a salt body on the heat flow and the base of GHSZ. The geometry of the salt body and the seabed topography are obtained from the 3D seismic data (Supplementary Figure 1A). Heat flow in the model occurs only through conduction, which assumes that heat advection due to pore fluid migration is negligible. The radiogenic heat, which produces heat in addition to the basal heat flow, is absent in salt and 1.0E-6 W/m^3 in the sediments[49].

The boundary conditions include a uniform temperature of 4.2°C at the seafloor, no heat flow at the side boundaries, and a uniform basal heat flow of 0.0234 W/m^2 (Supplementary Figure 1A). The basal heat flow is constrained by the seafloor temperature and regional average geothermal gradient of 25.5°C/km (see main text). The thermal conductivity of salt varies with temperature[37], ranging from ~5 W/m °C at the base of the salt body to ~7 W/m °C at the top of the model (Supplementary Figure 1B). The thermal conductivity of sediments (~1 to 2 W/m °C) is proportional to the porosity and the mineralogy, and the porosity decreases with depth according to observations in shallow marine sediments in the Gulf of Mexico [50] (Supplementary Figure 1C).

Transient 1D heat flow modeling

We use a numerical model[51] with a vertical grid size of 10 m to simulate the transient temperature change below the slide-impacted seafloor upon an instantaneous temperature change at the seafloor. At time 0, we set the temperature at the seafloor to 4.2°C and keep it constant with time; the base of the model is at the depth that is ~5 times the depth of the BSR, where there is a constant geothermal heat supply that correlates with the local geothermal gradients predicted by the 2D heat flow model. In addition, we assume the pores are fully saturated with water. The temperature is calculated from the energy conservation equation:

$$\frac{\partial \left[C_{bulk} T\right]}{\partial t} - \frac{\partial}{\partial z}\left[\lambda_{bulk} \frac{\partial T}{\partial z}\right] = 0,$$

1

where t is time (s); z is depth below the seafloor (m); T is temperature (°C); C_{bulk} is the bulk heat capacity (J kg^{-1} °C^{-1}) of the sediment; λ_{bulk} is the bulk thermal conductivity (W m^{-1} °C^{-1}). C_{bulk} and λ_{bulk} increase with depth as the porosity decreases (see supplementary material for the calculations of λ_{bulk} and C_{bulk} and physical properties of the sediments).

Analytical solution below slide escarpments

For more general cases, it is possible to assume homogeneous sediment properties and a constant geothermal heat flux below the slide escarpments. By solving equation (1) with constant λ_{bulk} and C_{bulk} we obtain an analytical expression for the depth evolution of the GHSZ (z_{bsr}, m) with a known temperature at the BHSZ (T_{bsr}, °C) [52]:

$$\frac{T_{bsr}-T_{z,0}}{T_{s,1}-T_{s,0}} = erfc\left(\frac{z_{bsr}}{2\sqrt{\kappa t}}\right), \quad (2)^{52}$$

where $T_{s,0}$ and $T_{s,1}$ are the seafloor temperature before and after the change, respectively (°C); $T_{z,0}$ is the initial temperature below the seafloor at depth z (°C) (see Figure 4A); T_{bsr} can be derived from the modern BSR depth (the intersection between the in situ temperature profile and the methane hydrate phase boundary) (see Figure 4A); κ is the average thermal diffusivity of the subseafloor sediment (see supplementary material); t is time.

Data Availability

The 3D seismic data are not publicly available due to its proprietary status. The data that support the findings of this study may be available on request from the corresponding author A.P.

Declarations

Acknowledgements

This work is supported by U.S. Department of Energy under contract DE-FE0023919. For our seismic interpretation we used a seismic volume provided by WesternGeco. We thank Manasij Santra for providing the geometry of the salt body used in the 2D heat flow modeling.

Author contributions

A.P. developed the idea that led to the paper, interpreted seismic data, and designed the figures. K.Y. and A.P. applied 1D transient heat flow and gas hydrate stability zone modeling. M.H. provided 2D conductive heat flow model. D.E.S. provided the porosity profiles. P.B.F., A.E.C. and K.Y. advised on the study's scope and conception. A.P. wrote the original manuscript, all authors contributed to the editing of the manuscript.

Competing interests

The authors declare no competing interests

References

1. Mienert, J. *et al.* Ocean warming and gas hydrate stability on the mid-Norwegian margin at the Storegga Slide. *Mar. Pet. Geol.* **22**, 233–244 (2005).
2. Maslin, M., Owen, M., Day, S. & Long, D. Linking continental-slope failures and climate change: Testing the clathrate gun hypothesis. *Geology* **32**, 53–56 (2004).
3. Masson, D. G., Harbitz, C. B., Wynn, R. B., Pedersen, G. & Løvholt, F. Submarine landslides: Processes, triggers and hazard prediction. *Philos. Trans. R. Soc. A Math. Phys. Eng. Sci.* **364**, 2009–2039 (2006).
4. Locat, J. & Lee, H. J. Submarine landslides: advances and challenges. https://doi.org/10.1139/*t01-089* **39**, 193–212 (2011).
5. Talling, P. J. *et al.* Large submarine landslides on continental slopes: Geohazards, methane release, and climate change. *Oceanography* **27**, 32–45 (2014).
6. Harbitz, C. B., Lovholt, F., Pedersen, G., Glimsdal, S. & Masson, D. G. Mechanisms of tsunami generation by submarine landslides - a short review. *Nor. J. Geol.* **86**, 255–264 (2006).
7. Carter, L. R., Gavey, R., Talling, P. J. & Liu, J. T. Insights into submarine geohazards from breaks in subsea telecommunication cables. *Oceanography* **27**, 58–67 (2014).
8. Berndt, C., Brune, S., Nisbet, E., Zschau, J. & Sobolev, S. V. Tsunami modeling of a submarine landslide in the Fram Strait. *Geochemistry, Geophys. Geosystems* **10**, (2009).
9. Posamentier, H. W. & Martinsen, O. J. The Character and Genesis of Submarine Mass-Transport Deposits: Insights from Outcrop and 3D Seismic Data. *Mass-Transport Depos. Deep. Settings* 7–38 (2011) doi:10.2110/SEPMSP.096.007.
10. Tappin, D. R. Submarine Landslides and Their Tsunami Hazard. *https://doi.org/*10.1146/annurev-earth-063016-015810 **49**, 551–578 (2021).
11. Hampton, M. A., Lee, H. J. & Locat, J. Submarine landslides. *Rev. Geophys.* **34**, 33–59 (1996).
12. Urlaub, M., Talling, P. J. & Masson, D. G. Timing and frequency of large submarine landslides: Implications for understanding triggers and future geohazard. *Quat. Sci. Rev.* **72**, 63–82 (2013).
13. Brothers, D. S., Luttrell, K. M. & Chaytor, J. D. Sea-level–induced seismicity and submarine landslide occurrence. *Geology* **41**, 979–982 (2013).
14. Pope, E. L. *et al.* Are large submarine landslides temporally random or do uncertainties in available age constraints make it impossible to tell? *Mar. Geol.* **369**, 19–33 (2015).
15. Lee, H. J. Timing of occurrence of large submarine landslides on the Atlantic Ocean margin. *Mar. Geol.* **264**, 53–64 (2009).
16. Haacke, R. R., Westbrook, G. K. & Hyndman, R. D. Gas hydrate, fluid flow and free gas: Formation of the bottom-simulating reflector. *Earth Planet. Sci. Lett.* **261**, 407–420 (2007).

17. Shipley, T. H. *et al.* Seismic Evidence for Widespread Possible Gas Hydrate Horizons on Continental Slopes and Rises. *Am. Assoc. Pet. Geol. Bull.* **63**, 2204–2213 (1979).
18. Kvenvolden, K. A. Gas hydrates-geological perspective and global change. *Rev. Geophys.* **31**, 173–187 (1993).
19. Ruppel, C. & Kessler, J. D. The Interaction of Climate Change and Methane Hydrates. *Rev. Geophys.* 1–43 (2016) doi:10.1002/2016RG000534.
20. Kvenvolden, K. A. & Lorenson, T. D. The Global Occurrence of Natural Gas Hydrate. *Nat. Gas Hydrates Occur. Distrib. Detect.* 3–18 (2001) doi:10.1029/GM124p0003.
21. Phrampus, B. J., Harris, R. N. & Tréhu, A. M. Heat flow bounds over the Cascadia margin derived from bottom simulating reflectors and implications for thermal models of subduction. *Geochemistry, Geophys. Geosystems* **18**, 3309–3326 (2017).
22. Shedd, W., Boswell, R., Frye, M., Godfriaux, P. & Kramer, K. Occurrence and nature of ‘ bottom simulating reflectors’ in the northern Gulf of Mexico. *Mar. Pet. Geol.* **34**, 31–40 (2012).
23. Smith, A. J., Mienert, J., Bünz, S. & Greinert, J. Thermogenic methane injection via bubble transport into the upper Arctic Ocean from the hydrate-charged Vestnesa Ridge, Svalbard. *Geochemistry, Geophys. Geosystems* **15**, 1945–1959 (2014).
24. Portnov, A., Cook, A. E. & Vadakkepuliyambatta, S. Diverse gas composition controls the Moby-Dick gas hydrate system in the Gulf of Mexico. *Geology* (2021) doi:10.1130/G49310.1.
25. Ruppel, C., Dickens, G. R., Castellini, D. G., Gilhooly, W. & Lizarralde, D. Heat and salt inhibition of gas hydrate formation in the northern Gulf of Mexico. *Geophys. Res. Lett.* **32**, (2005).
26. Posewang, J. & Mienert, J. The enigma of double BSRs: Indicators for changes in the hydrate stability field? *Geo-Marine Lett.* **19**, 157–163 (1999).
27. Andreassen, K., Mienert, J., Bryn, P. & Singh, S. C. A double gas-hydrate related bottom simulating reflector at the Norwegian continental margin. in *Annals of the New York Academy of Sciences* vol. 912 126–135 (New York Academy of Sciences, 2000).
28. Lee, G. H., Kim, H. J., Jou, H. T. & Cho, H. M. Opal-A/opal-CT phase boundary inferred from bottom-simulating reflectors in the southern South Korea Plateau, East Sea (Sea of Japan). *Geophys. Res. Lett.* **30**, 1–4 (2003).
29. Han, S. *et al.* The many double BSRs across the northern Hikurangi margin and their implications for subduction processes. *Earth Planet. Sci. Lett.* **558**, 116743 (2021).
30. Pecher, I. A. *et al.* A Fluid Pulse on the Hikurangi Subduction Margin: Evidence From a Heat Flux Transect Across the Upper Limit of Gas Hydrate Stability. *Geophys. Res. Lett.* **44**, 12,385-12,395 (2017).
31. Zander, T. *et al.* On the origin of multiple BSRs in the Danube deep-sea fan, Black Sea. *Earth Planet. Sci. Lett.* **462**, 15–25 (2017).
32. Shokes, R. F., Trabant, P. K., Presley, B. J. & Reid, D. F. Anoxic, Hypersaline Basin in the Northern Gulf of Mexico. *Science (80-.).* **196**, 1443–1446 (1977).

33. Sawyer, D. E., Mason, R. A., Cook, A. E. & Portnov, A. Submarine Landslides Induce Massive Waves in Subsea Brine Pools. *Sci. Rep.* **9**, (2019).
34. Pilcher, R. S. & Blumstein, R. D. Brine volume and salt dissolution rates in Orca Basin, northeast Gulf of Mexico. *Am. Assoc. Pet. Geol. Bull.* **91**, 823–833 (2007).
35. Hillman, J. I. T., Cook, A. E., Sawyer, D. E., Küçük, H. M. & Goldberg, D. S. The character and amplitude of 'discontinuous' bottom-simulating reflections in marine seismic data. *Earth Planet. Sci. Lett.* **459**, (2017).
36. Kramer, K. V & Shedd, W. W. A 1.4-billion-pixel map of the Gulf of Mexico seafloor. *Earth Sp. Sci. News* **98**, (2017).
37. Mello, U. T., Karner, G. D. & Anderson, R. N. Role of salt in restraining the maturation of subsalt source rocks. *Mar. Pet. Geol.* **12**, 697–716 (1995).
38. Hornbach, M. J., Ruppel, C., Saffer, D. M., Van Dover, C. L. & Holbrook, W. S. Coupled geophysical constraints on heat flow and fluid flux at a salt diapir. *Geophys. Res. Lett.* **32**, (2005).
39. Portnov, A. *et al.* Salt-driven evolution of a gas hydrate reservoir in Green Canyon, Gulf of Mexico. *Am. Assoc. Pet. Geol. Bull.* **104**, 1903–1919 (2020).
40. Donoghue, J. F. Sea level history of the northern Gulf of Mexico coast and sea level rise scenarios for the near future. *Clim. Change* **107**, 17–33 (2011).
41. Handa, Y. P. Compositions, enthalpies of dissociation, and heat capacities in the range 85 to 270 K for clathrate hydrates of methane, ethane, and propane, and enthalpy of dissociation of isobutane hydrate, as determined by a heat-flow calorimeter. *J. Chem. Thermodyn.* **18**, 915–921 (1986).
42. Hill, J. C. *et al.* Subsurface controls on the development of the Cape Fear Slide Complex, central US Atlantic Margin. *Geol. Soc. London, Spec. Publ.* **477**, 169–181 (2019).
43. Lenz, B. L., Sawyer, D. E., Phrampus, B., Davenport, K. & Long, A. Seismic Imaging of Seafloor Deformation Induced by Impact from Large Submarine Landslide Blocks, Offshore Oregon. *Geosci.* 2019, *Vol. 9, Page 10* **9**, 10 (2018).
44. Bünz, S., Mienert, J. & Berndt, C. Geological controls on the Storegga gas-hydrate system of the mid-Norwegian continental margin. *Earth Planet. Sci. Lett.* **209**, 291–307 (2003).
45. Gee, M. J. R., Uy, H. S., Warren, J., Morley, C. K. & Lambiase, J. J. The Brunei slide: A giant submarine landslide on the North West Borneo Margin revealed by 3D seismic data. *Mar. Geol.* **246**, 9–23 (2007).
46. Geissler, W. H. *et al.* Arctic megaslide at presumed rest. *Sci. Rep.* **6**, 38529 (2016).
47. Vanneste, M., Mienert, J. & Bünz, S. The Hinlopen Slide: A giant, submarine slope failure on the northern Svalbard margin, Arctic Ocean. *Earth Planet. Sci. Lett.* **245**, 373–388 (2006).
48. Sloan, E. D. & Koh, C. A. *Clathrate Hydrates of Natural Gases, Third Edition*. *Clathrate Hydrates of Natural Gases, Third Edition* (CRC Press, 2008). doi:doi:10.1201/9781420008494.fmatt 10.1201/9781420008494.fmatt.

49. Christie, C. H. & Nagihara, S. Geothermal gradients of the northern continental shelf of the Gulf of Mexico. *Geosphere* **12**, 26–34 (2016).
50. Christie, C. H. & Nagihara, S. Geothermal gradients of the northern continental shelf of the Gulf of Mexico. *Gulf Mex. Geosph.* / **12**, (2015).
51. You, K. & Flemings, P. B. Methane Hydrate Formation in Thick Sandstones by Free Gas Flow. *J. Geophys. Res. Solid Earth* **123**, 4582–4600 (2018).
52. Turcotte, D. L. & Schubert, G. Geodynamics. (2002) doi:10.1017/CBO9780511807442.

Figures

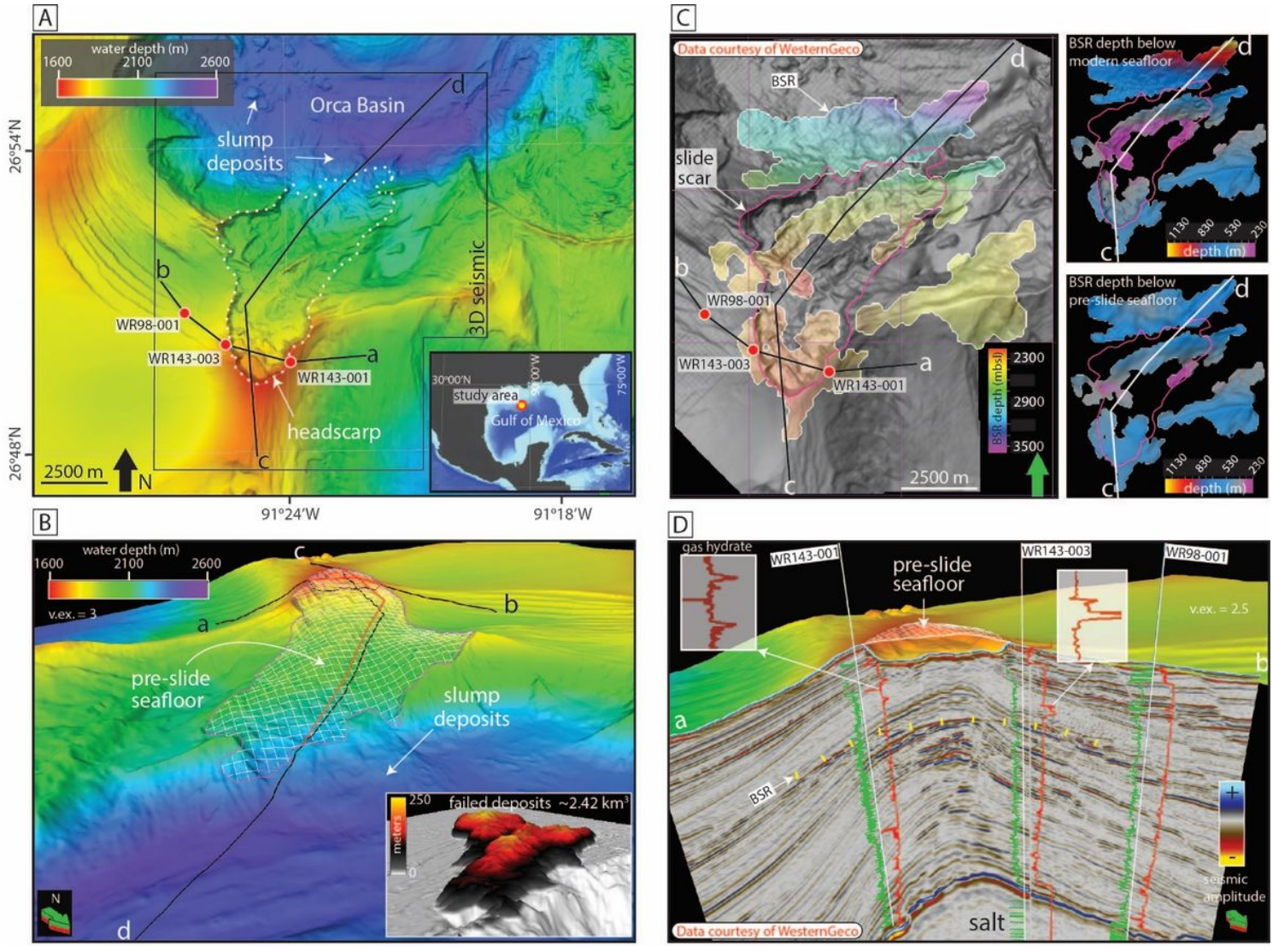

Figure 1

Orca submarine landslide and bottom simulating reflections (BSR) in the 3D seismic data. A) Seafloor bathymetry36 showing the submarine slide escarpment (white dotted line) in the Orca Basin, Gulf of Mexico (see inset for location of the study area). B) Reconstructed pre-slide bathymetry and the estimated volume of the failed deposits in the inset. C) Colored areas in the big panel show the BSR

extent and depth (mbsl). Pink line outlines the slide escarpment over the gray shaded bathymetry surface. The two panels on the right show the highly variable BSR depth below the modern seafloor (upper) and more coherent BSR depth below the reconstructed pre-slide seafloor (lower). D) Seismic cross section a-b shows three industry wells (labeled white lines) with plotted gamma ray (green) and resistivity (red) logs. Location of the cross section is shown in Figure 1A, B, C. Gas hydrates are evident from the high-resistivity intervals above the BSR in the wells WR143-001 and WR143-003.

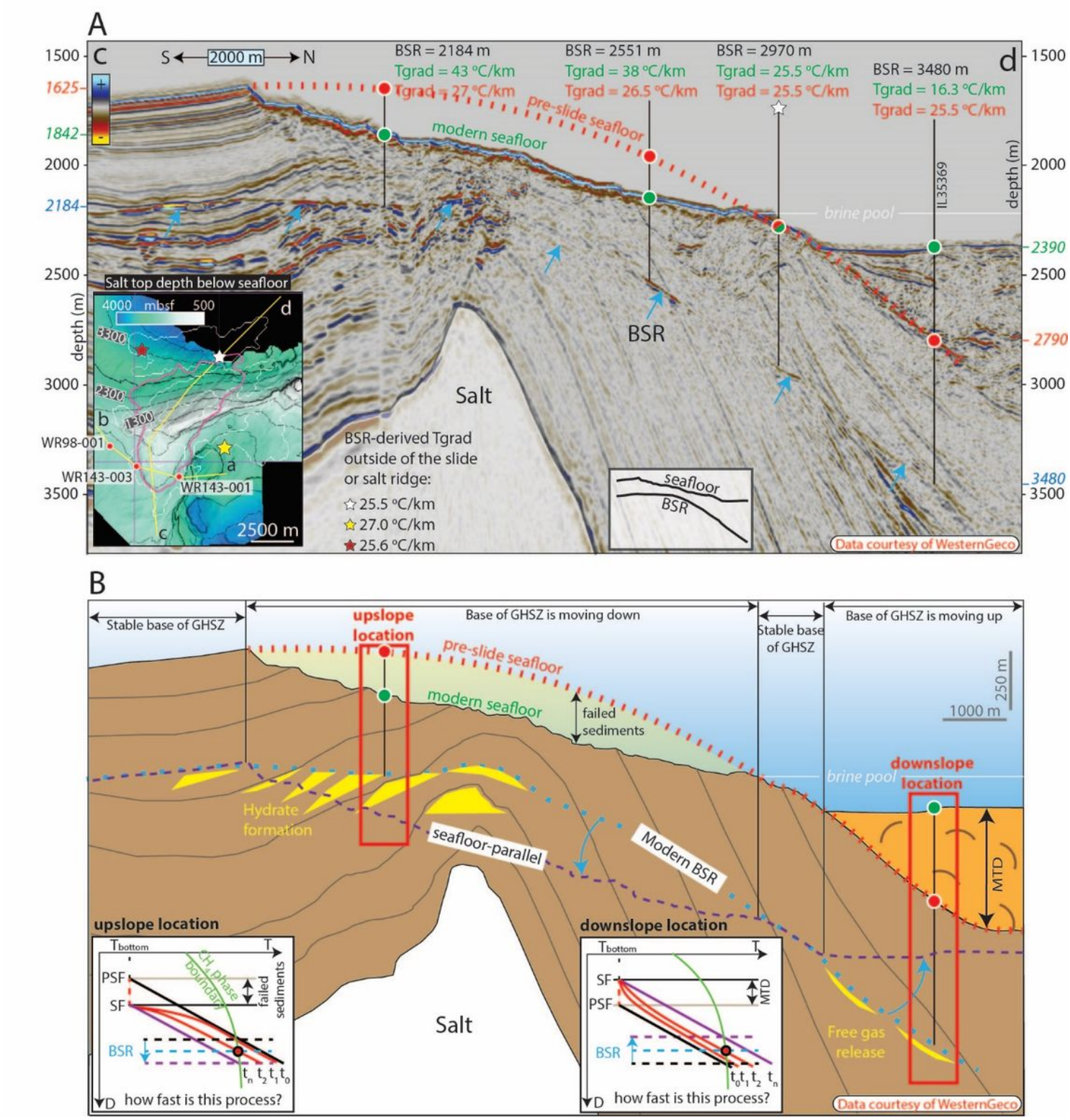

Figure 2

Irregular bottom simulating reflection (BSR) under the slide-impacted seafloor. A) Seismic cross-section c-d showing the BSR, which is not parallel to the modern seafloor (blue arrows), but strikingly parallel to the reconstructed pre-slide seafloor (red dotted line). Steady-state geothermal gradients required to explain the depth of the bottom simulating reflection (BSR) using pre-slide seafloor (red) show better consistency than those calculated using the BSR and modern seafloor depths (green); Tgrad-geothermal gradient. The left inset shows three BSR locations (stars) outside of the slide escarpment (pink line) and away from the shallow salt (colored surface in mbsf) selected for calculation of the regional average geothermal gradient in our study area (25.5 °C/km). B) Interpreted seismic section c-d showing the pre-slide seafloor, modern BSR, mass transport deposits (MTD), upslope and downslope locations selected for modeling analyses and other elements of the slide-gas hydrate system labeled. Insets show schematic adjustment of the temperature field after the slope failure (cooling effect at the upslope location and warming effect at the downslope location) leading to the reciprocal BSR shifts (blue arrows). SF-seafloor; PSF – pre-slide seafloor; T-temperature; D-depth; t0-n -time-temperature profiles.

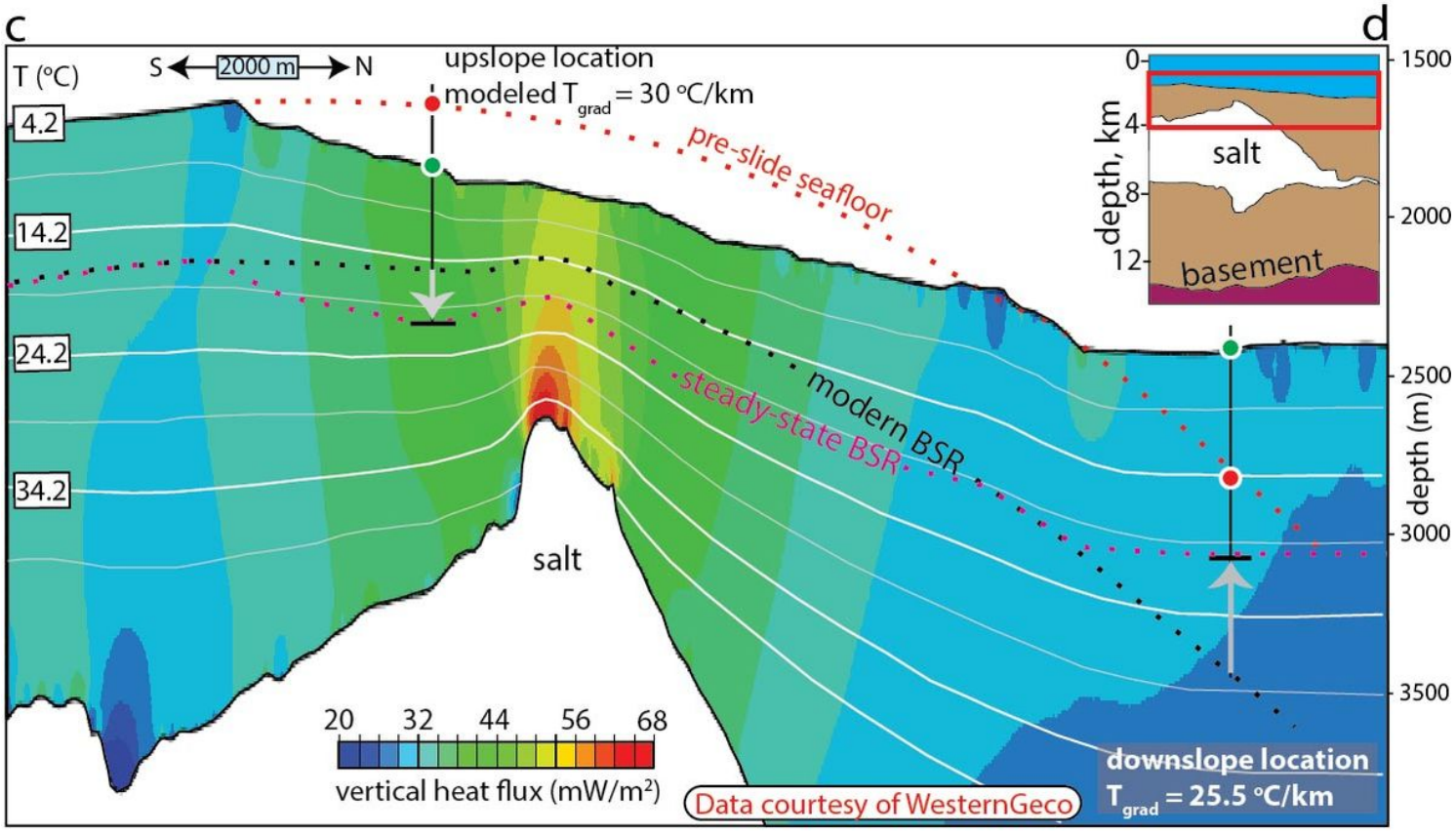

Figure 3

Two-dimensional steady-state conductive heat flow model.

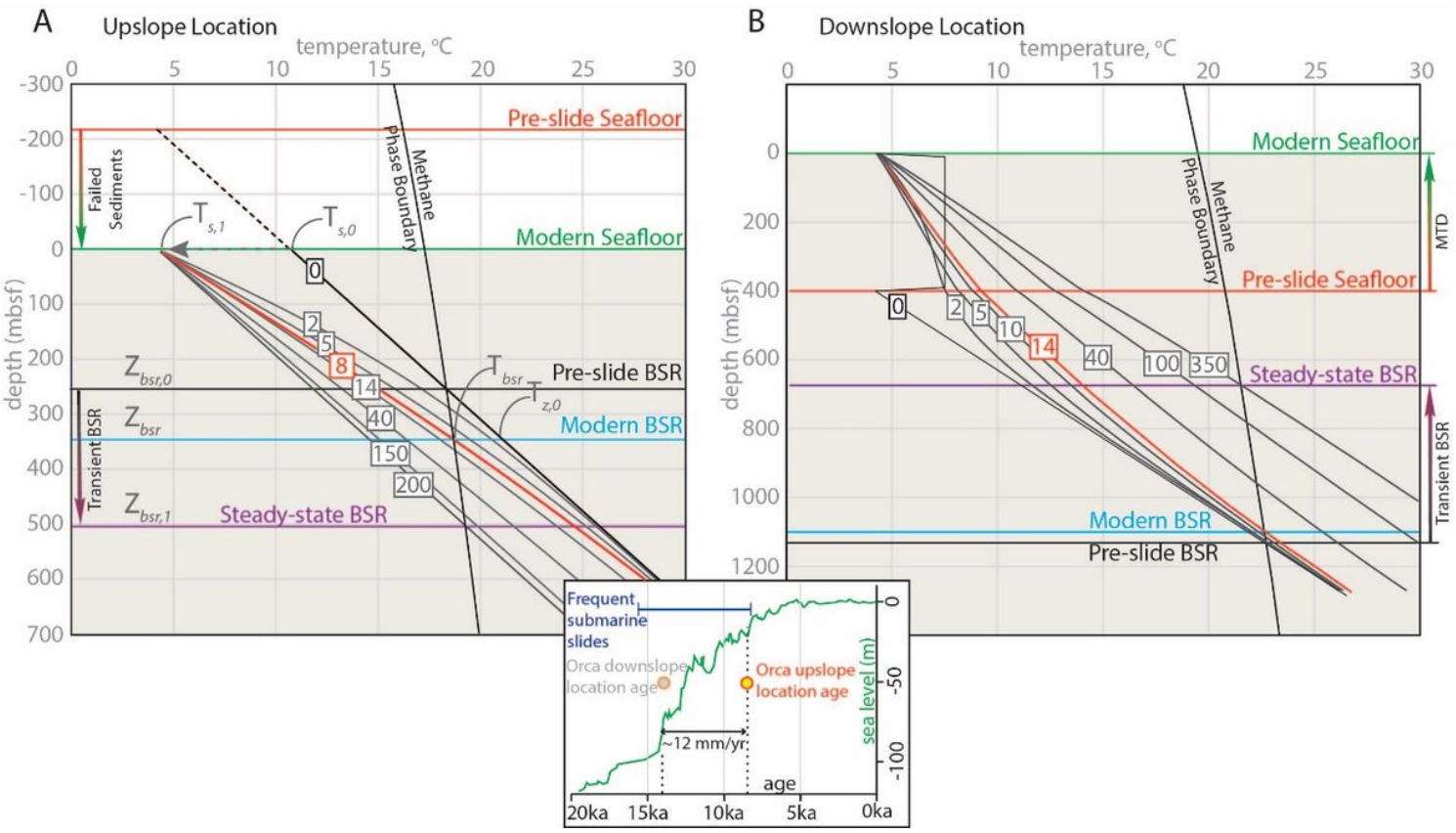

Figure 4

Transient 1D heat flow modeling at the upslope and downslope locations.

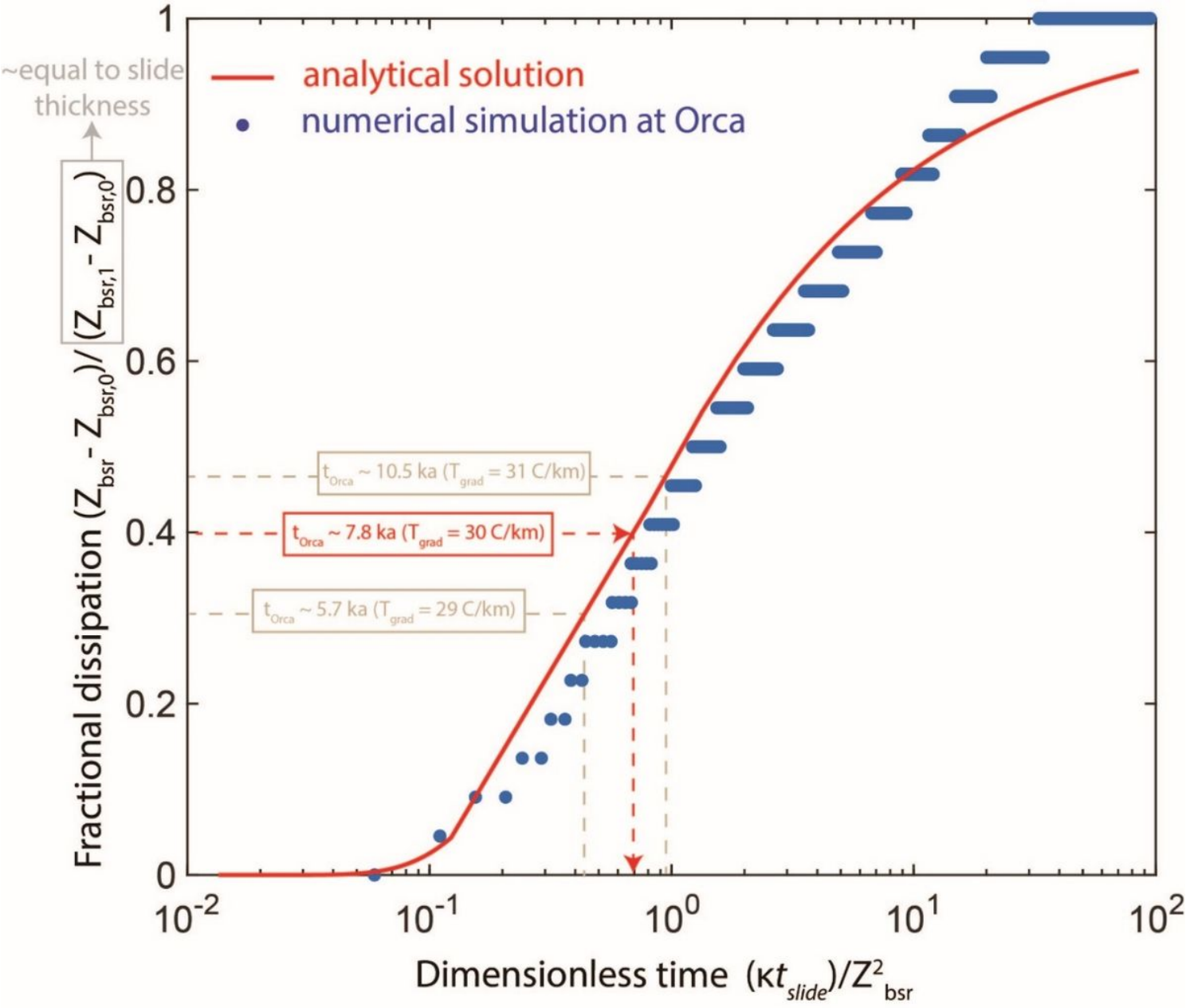

Figure 5

Analytical solution for submarine landslide dating.

Supplementary Files

This is a list of supplementary files associated with this preprint. Click to download.

- Supplementaryinformation.docx